

RESEARCH ARTICLE | DECEMBER 19 2025

## Laser system for frequency domain velocimetry and atom interferometry experiments

J. Randhawa   ; G. Carlse  ; M. B. Llaguno  ; J. Cuzzupoli  ; E. Chomen Ramos  ; T. Vacheresse  ; A. Pouilot  ; A. Kumarakrishnan 



*Rev. Sci. Instrum.* 96, 123204 (2025)

<https://doi.org/10.1063/5.0301085>



### Articles You May Be Interested In

Characterization and applications of auto-locked vacuum-sealed diode lasers for precision metrology

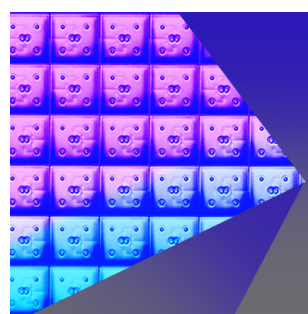
*Rev. Sci. Instrum.* (August 2019)

Measuring the effective height for atom gravimeters by applying a frequency jump to Raman lasers

*Rev. Sci. Instrum.* (June 2021)

The Collective Atomic Recoil Laser

*AIP Conf. Proc.* (May 2005)



**Review of  
Scientific Instruments**  
**Special Topics Now Online**

[Learn More](#)

 **AIP  
Publishing**

# Laser system for frequency domain velocimetry and atom interferometry experiments

Cite as: Rev. Sci. Instrum. 96, 123204 (2025); doi: 10.1063/5.0301085

Submitted: 5 September 2025 • Accepted: 3 December 2025 •

Published Online: 19 December 2025



View Online



Export Citation



CrossMark

J. Randhawa,<sup>a)</sup> G. Carlse, M. B. Llaguno, J. Cuzzupoli, E. Chomen Ramos, T. Vacheresse, A. Pouliot, and A. Kumarakrishnan<sup>b)</sup>

## AFFILIATIONS

Department of Physics and Astronomy, York University, 4700 Keele Street, Toronto, Ontario M3J 1P3, Canada

<sup>a)</sup>Author to whom correspondence should be addressed: [jr28@my.yorku.ca](mailto:jr28@my.yorku.ca)

<sup>b)</sup>[akumar@yorku.ca](mailto:akumar@yorku.ca)

## ABSTRACT

We discuss the characterization and specifications of a home-built external cavity diode laser system that is suitable for frequency-domain cold-atom velocimetry and measurements of gravitational acceleration. The laser system is frequency stabilized using a modulation-free technique that lowers the temperature of a magneto-optical trap (MOT) in comparison with a MOT realized using a laser that relies on lock-in spectroscopy. The laser system also incorporates a feedback loop involving an acousto-optic modulator for intensity stabilization, which reduces the effect of low frequency vibrations. By integrating this laser with a home-built, dual-output radio frequency synthesizer, we are able to derive two laser beams with a precisely controlled relative detuning for frequency domain interferometry using laser-cooled atoms. The detuning can range from the mHz to the MHz level with a stability of 10  $\mu$ Hz.

Published under an exclusive license by AIP Publishing. <https://doi.org/10.1063/5.0301085>

## I. INTRODUCTION

The rapid advancement of the field of precision metrology using ultra-cold atoms to develop quantum sensors is based in part on the realization of highly integrated and prefabricated setups that are used in tabletop experiments and in the development of portable instrumentation and large-scale experiments, such as atomic fountains, atomic clocks, and drop towers that are used for atom interferometry.<sup>1–7</sup> Nevertheless, even sophisticated experiments can benefit from simple techniques that can be validated using small-scale laboratory setups that involve home-built devices. In this context, there is a long record of foundational techniques and proof-of-concept experiments that have relied on narrow-linewidth external cavity diode lasers (ECDLs).<sup>8–20</sup> This paper focuses on applications of a particular class of ECDLs that rely on interference filter (IF) stabilized cavities,<sup>8,19,20</sup> which have proven to be easily adaptable for varied applications in precision metrology.

In previous work,<sup>8</sup> we showed that an IF-stabilized, vacuum-sealable laser system equipped with a low-noise current controller was suitable for state-of-the-art industrial gravimetry and for developing differential absorption LIDAR transmitters. This laser system relied on either traditional lock-in spectroscopy or an

auto-locking, pattern-matching, digital controller for frequency stabilization. Under these conditions, the stability of the laser was characterized by an Allan Deviation (ADEV) with a floor as low as  $2 \times 10^{-12}$  at 300 s, which is comparable to a commercial rubidium atomic clock typically yielding an ADEV floor less than  $2 \times 10^{-12}$  at 100 s.<sup>21</sup> This laser system is suitable for accurate measurements of atomic diffusion coefficients using coherent scattering techniques, measurements that constitute the basis of a quantum pressure sensor,<sup>22,23</sup> measurements of atomic lifetimes using photon echoes,<sup>24</sup> and optical tweezers experiments to measure masses of microparticles.<sup>25</sup>

However, the development of cold-atom sensors for velocimetry and gravimetry based on atom interferometers<sup>26–28</sup> impose more stringent requirements, such as linewidth control for minimizing the temperature of the sample and for deriving the excitation beams with precisely controlled relative detunings. In this paper, we show that it is possible to realize a reconfigured laser system based on our previous work<sup>8</sup> using specialized feedback loops and radio frequency (RF) electronics to achieve these goals.

In the first part of this paper, we demonstrate the impact of laser frequency stabilization using a modulation-free feedback system that reduces the temperature of a laser-cooled atomic sample. Examples

of such modulation-free systems include the Dichroic Atomic Vapor Laser Lock (DAVLL),<sup>29–31</sup> the Doppler-Free version of this scheme (DF-DAVLL),<sup>18,32–37</sup> and feedback loops that rely on electro-optic modulators (EOMs)<sup>38,39</sup> and acousto-optic modulators (AOMs).<sup>40</sup> In all these experiments, differential absorption is used to produce a dispersion-shaped error signal in a sidearm containing a saturated absorption spectrometer.<sup>41</sup> Although all these schemes have particular advantages and they realize lasers with suitable frequency stability, their effect on atomic samples does not seem to have been sufficiently explored. Here, we rely on the DF-DAVLL scheme<sup>18,32–37</sup> for frequency stabilization and demonstrate a systematic reduction in the temperature of a magneto-optical trap (MOT) in comparison with the sample temperature obtained using an ECDL frequency stabilized using lock-in spectroscopy. To make this comparison, we rely on the correlation between the laser linewidth and the MOT temperature. We establish this correlation by increasing the laser linewidth using the modulation amplitude of the lock-in controller.

In the second part, we focus on another desirable feature of this laser system for cold-atom interferometry experiments in a typical laboratory environment with acoustic noise, namely, laser intensity stabilization. Work by Savard *et al.*<sup>42</sup> highlighted the role of intensity stabilization in far off resonance traps (FORTs), but this aspect does not seem to have been studied extensively in the context of MOTs. In our work, we find that a simple feedback circuit based on an AOM and RF electronics is effective in suppressing laser intensity fluctuations arising from low-frequency vibrations.

In the final part of the paper, we show that this laser can be integrated with a low-cost, home-built, dual-output frequency synthesizer for single-state atom interferometric measurements of the velocity and gravitational acceleration of a cold-atom sample.<sup>26–28</sup> This synthesizer enables fine control over the relative detuning between two laser beams that originate from the same laser source. We demonstrate a tuning range of 1 mHz–1 MHz for this relative detuning and stability at the level of 10  $\mu$ Hz. We also show that

the laser intensity stabilization feedback loop can be reconfigured to ensure the power stability of the RF output over the tuning range of several MHz.

In what follows, we organize the paper into an experimental section (Sec. II) that describes the layout of the DF-DAVLL frequency stabilization scheme, the setup for the comparative MOT temperature measurements, the schematic of the circuit used for laser intensity and RF power stabilization, followed by the RF network for the dual output synthesizer. In the subsequent section (Sec. III), we describe the data relating to the frequency stability of the laser system, results of intensity stabilization, comparative cold-atom temperature measurements, and performance characteristics of the RF synthesizer.

## II. EXPERIMENTAL SETUP

### A. Doppler-free dichroic atomic vapor laser lock (DF-DAVLL)

The Doppler-Free Dichroic Atomic Vapor Laser Lock (DF-DAVLL) system is shown in Fig. 1.<sup>18,32–37</sup> A home-built ECDL operating at 780 nm<sup>8</sup> is locked to the  $5S_{1/2} F = 3 \rightarrow 5P_{3/2} F' = 2, 4$  crossover peak in  $^{85}\text{Rb}$ . A small fraction of the laser power output is used to generate linearly polarized, counter-propagating pump and probe laser beams that are aligned through a rubidium vapor cell at room temperature that has a length of 5 cm. The cell is placed within a solenoid capable of generating magnetic fields up to 50 G. The differential absorption of opposite circularly polarized components of the probe light is recorded in the presence of a 10–20 G magnetic field on a balanced detector (PD-A and PD-B in Fig. 1) using a quarter wave-plate and a polarizing beam splitter located after the vapor cell. The output of this balanced detector provides a dispersion-shaped error signal. Using a home-built PID controller, this error signal is filtered and sent to both the ECDL current and a piezo-controlled mirror in the laser

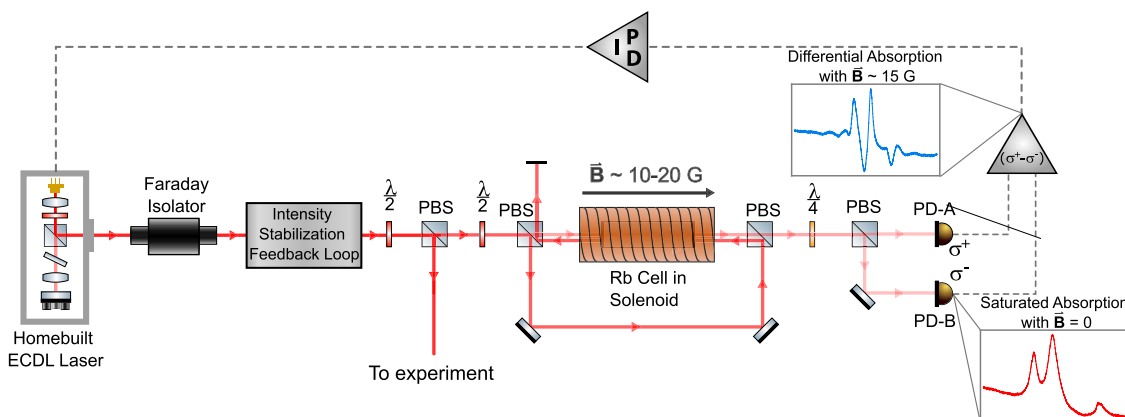


**FIG. 1.** Optical setup of the Doppler-Free Dichroic Atomic Laser Lock (DF-DAVLL) system. Light from a home-built ECDL (output of ~60 mW) is split using a half-wave plate ( $\lambda/2$ ) and a polarizing beam splitting (PBS) cube to send most of the light to the atom trapping experiment through an optical fiber and a small fraction to the DF-DAVLL setup. The saturated absorption from the rubidium vapor cell detected by a single photodiode (PD-B) is shown in the red inset in the absence of the magnetic field. The differential absorption (shown in the blue inset) in the presence of a magnetic field due to the Zeeman shift is recorded using two photodiodes (PD-A and PD-B) and a subtractor circuit. The magnetic field is generated by a two-layered solenoid of length 16 cm, radius 2.5 cm, and  $\approx 150$  turns. Multiple Faraday isolators with a total extinction ratio of 75 dB were used to isolate the ECDL from optical feedback. An intensity stabilization feedback loop is included in the setup. This feedback loop includes an AOM and it reduces the amplitude of laser intensity fluctuations by a factor of  $\approx 3$ .

cavity to stabilize the frequency of the laser to the desired lock point. To amplify the light from the ECDL, we rely on the use of a 2 W semi-conductor waveguide tapered amplifier<sup>43</sup> to generate the trapping beams for the MOT. We note that it is well established that tapered amplifiers replicate the spectral properties of the seed light.<sup>44,45</sup>

## B. Laser intensity stabilization feedback loop

In Fig. 1, the ECDL and DF-DAVLL setups are placed on a sub-Hertz vibration isolation platform with a resonant frequency of  $\sim 1$  Hz. Since this setup is coupled to several sources of acoustic vibrations ranging up to several kHz, such as fans, motors, and mechanical pumps, we observed intensity noise at characteristic frequencies, such as table resonances in the lock signal. Therefore, we introduced an intensity stabilization feedback loop in the laser beam directed toward the DF-DAVLL setup. The details of this setup, which includes an AOM, are shown in Fig. 2. The light from the ECDL is incident on an AOM and the diffracted beam is split off by a beam splitter and detected by a photodiode with a rise time of 10 ns. The photodiode signal serves as the input to an analog circuit, whose details are shown in Fig. 3. This circuit generates a feedback voltage to control the RF power level of the AOM using a voltage-controlled attenuator (VCA) with a response time of 14  $\mu$ s and a bandwidth of 10–2500 MHz. Examples of AOM-based intensity stabilization feedback loops are described in Refs. 46–49.

We now describe the details of the analog stabilization circuit shown in Fig. 3. This circuit consists of three stages. In the first stage, the photodiode input is compared to a variable setpoint voltage using a subtractor to generate an error signal. In the second stage, a proportional gain amplifier and integrator with a time constant ranging from 100  $\mu$ s to 100 ms are used to generate a correction signal. In the third stage, the correction signal is added to an offset voltage (DC adjust) using a summing amplifier. The resulting signal is designed to match the control voltage range of the VCA (0–15 V) that controls the RF power level to the AOM.

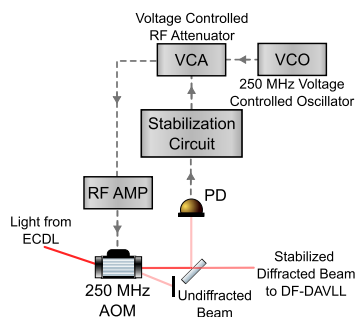


**FIG. 2.** Feedback loop for intensity stabilization. Light from the ECDL is coupled through an AOM operating at 250 MHz and driven by a RF amplifier (RF AMP) whose power output is controlled by a voltage-controlled attenuator (VCA). The primary input to the RF amplifier is the signal from a voltage-controlled oscillator (VCO). The diffracted beam from the AOM, which is directed to the DF-DAVLL setup in Fig. 1, is intensity stabilized. A small fraction of this beam intensity is incident on a photodiode in a sidearm. The signal from the photodiode is the input for an analog stabilization circuit. The correction signal generated by this circuit controls the RF power to the AOM.

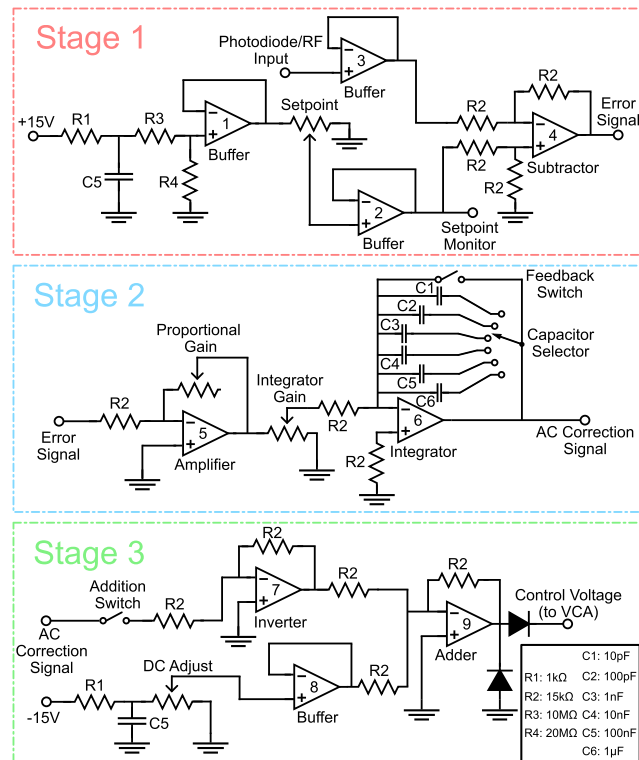


**FIG. 3.** Analog circuit for laser intensity stabilization. In stage 1, the photodiode input is compared with a setpoint voltage to generate an error signal. In stage 2, the error signal is amplified and integrated to generate a correction voltage. In stage 3, the correction signal is added to an offset voltage to generate the control voltage for the RF attenuator. A diode connected to ground is used to isolate the RF attenuator from large negative voltages and a second diode is used to protect the circuit from unwanted feedback.

## C. Comparative measurements of MOT temperature

We rely on the measurements of MOT temperature to quantify the effects of frequency modulation. The MOT temperature is measured using CCD photography of time-of-flight expansion of the atomic cloud.<sup>50</sup> Comparative measurements are carried out using two separate lasers to seed a tapered amplifier used to generate the MOT trapping beams as shown in Fig. 4. The seed laser is either an ECDL that is frequency stabilized using a lock-in amplifier or the laser system used in this work, which is an IF laser stabilized using the DF-DAVLL technique. These measurements also allow us to quantify the effect of heating by increasing the characteristic modulation amplitude of the lock-in stabilized laser. For the temperature measurements, the output of the tapered amplifier is aligned through a dual-pass AOM that controls the trapping beams. The atoms are cooled by polarization gradient cooling using this AOM as described by the procedure in our previous work.<sup>51</sup>

## D. Dual-output, tunable radio frequency synthesizer

For single-state, frequency domain atom interferometry, we rely on the use of a home-built RF synthesizer to produce the necessary excitation pulses required for measurements of velocity and

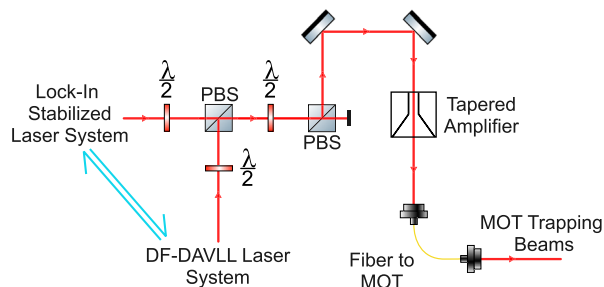


**FIG. 4.** Optical setup for comparative measurements of MOT temperature using two seed lasers. Either a lock-in stabilized seed laser or a modulation-free seed laser is used to seed a tapered waveguide amplifier with the same input polarization using a half-wave plate ( $\lambda/2$ ) and polarizing beam splitting cube (PBS). The amplifier's output is fiber-coupled into three orthogonal trapping beams.

gravitational acceleration. This synthesizer produces two outputs used to drive separate AOMs at the frequencies  $125 + \delta/2$  and  $125 - \delta/2$  MHz, where  $\delta$  is the detuning between the outputs. These AOMs derive light from a common laser source. The RF network is shown in Fig. 5. Instead of relying on two separate commercial RF synthesizers, our scheme uses an inexpensive phase-locked loop (PLL) operating at 100 MHz and two arbitrary waveform generators (AWG1 and AWG2) operating at 100 MHz.

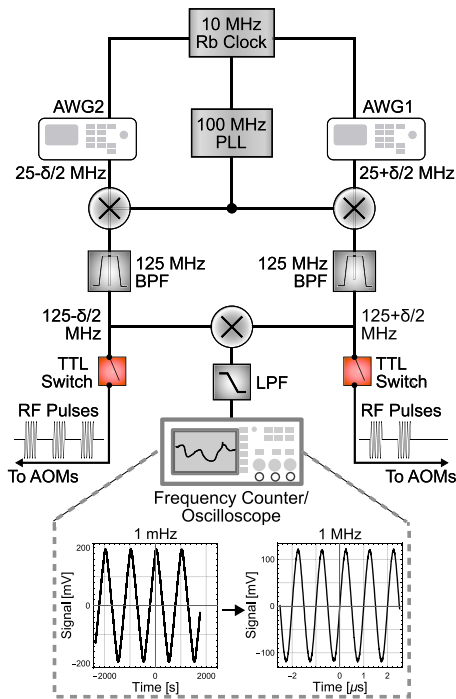


**FIG. 5.** RF synthesizer network used to generate two AOM outputs at  $125 + \delta/2$  and  $125 - \delta/2$  MHz, where  $\delta$  is a small detuning. Three oscillators, all referenced to a 10 MHz rubidium clock, are used to generate slightly detuned beat notes for driving the AOMs. One of the oscillators is derived from a 100 MHz phase-locked loop and the other two oscillators are derived from commercial arbitrary waveform generators (AWG1 and AWG2). The bandpass filters centered at 125 MHz and the TTL switches with an extinction ratio of  $\sim 90$  dB are used in the AOM drivers.

(AWGs) operating at  $25 + \delta/2$  and  $25 - \delta/2$  MHz. The frequency stability and accuracy of both AWG outputs rely on separate crystal oscillators that can be referenced to a 10 MHz rubidium clock of superior stability.<sup>21</sup> The same clock provides a reference to a PLL, which generates a stable output at 100 MHz. Since the PLL cannot be smoothly tuned despite its large tuning range, we rely on the versatility of the AWG outputs, which are tunable to 1  $\mu$ Hz. Each AWG output is mixed with the 100 MHz PLL output and filtered using a bandpass filter centered near 125 MHz to remove the difference frequency. The resultant outputs are sent to transistor-transistor logic (TTL) switches to produce RF pulses that are used to drive the AOMs that generate the mutually detuned, counter-propagating traveling wave pulses for atom interferometry.

To characterize the synthesizer, we measured the stability, tunability, and frequency response of the two outputs. To characterize the tunability and stability, the two RF outputs are mixed together and low-pass filtered to generate a beat note at the difference frequency,  $\delta$ . The beat note is monitored either on an oscilloscope to test tunability or on a frequency counter to test stability as illustrated in Fig. 5.

### III. RESULTS AND DISCUSSION

#### A. Laser frequency stability

We have characterized the laser frequency stability of the DF-DAVLL lock shown in Fig. 1. As shown in our previous work,<sup>8</sup> under carefully controlled laboratory conditions, the stability of the lock signal provides a comparable measure of performance compared to the beat note between two uncorrelated laser sources, which requires a more elaborate setup. Since laser performance is known to be limited by current noise,<sup>8</sup> we have recorded the lock stability using two different laser current controllers. The blue trace in Fig. 6 shows an ADEV noise floor of  $7 \times 10^{-12}$  at 30 s using a current controller with a power spectral density of  $100 \text{ pA}/\sqrt{\text{Hz}}$ . This dataset was acquired with a sampling rate of 16 kS/s and shows the Hz-level resonances of the vibration isolation platform. These results are somewhat worse than the ADEV floor of  $2 \times 10^{-12}$  at 300 s realized in previous work<sup>8</sup> using a wavelength-selected diode. We attribute the difference to modifications of the home-built control electronics. The green trace in Fig. 6 shows a higher ADEV noise floor of  $2.3 \times 10^{-11}$  at 150 s using a current controller with a power spectral density of  $480 \text{ pA}/\sqrt{\text{Hz}}$ . This dataset was acquired at a sampling rate of 1 kS/s. Since this controller is 20 times less expensive, it provides a reasonable solution for most applications without sacrificing stability. Figure 6 also shows the ADEV plot of the lock-in stabilized laser for comparison in purple. This dataset was acquired with a sampling rate of 1 kS/s using a current controller with a power spectral density of  $200 \text{ nA}/\sqrt{\text{Hz}}$ . Here, the ADEV floor is  $6.6 \times 10^{-13}$  at 30 s. We note that while the ADEV floor of this laser is significantly lower than the home-built lasers, the sampling rate does not show the influence of the 6 kHz modulation frequency. The data presented later in the paper reveals the impact of modulation on the temperature of cold atoms. The polynomial fits (in red) to all three datasets suggest that the dominant noise sources over short timescales are white phase noise ( $\tau^{-1}$ ) and white frequency noise ( $\tau^{-1/2}$ ). The white phase noise is indicative of noise from electronic circuits, and the white frequency noise is a generic feature

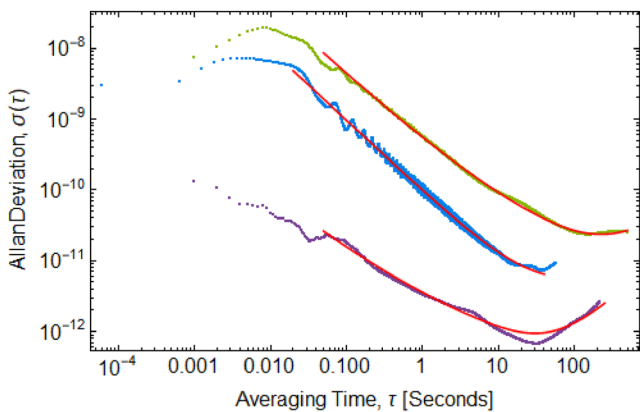


**FIG. 6.** Allan deviation of the lock signal of a DF-DAVLL stabilized laser measured using a current controller with a power spectral density of 100 pA/ $\sqrt{\text{Hz}}$  (blue), for which the fit function is  $(9.7 \times 10^{-11})\tau^{-1} + (8.8 \times 10^{-18})\tau^{-1/2} + (3.4 \times 10^{-12})\tau^0 + (2.1 \times 10^{-18})\tau^{1/2} + (1.6 \times 10^{-14})\tau^1$  and the floor is  $\approx 7 \times 10^{-12}$ . For a current controller with a power spectral density of 480 pA/ $\sqrt{\text{Hz}}$  (green), the fit function is  $(4.0 \times 10^{-10})\tau^{-1} + (1.6 \times 10^{-10})\tau^{-1/2} + (8.3 \times 10^{-19})\tau^0 + (5.6 \times 10^{-13})\tau^{1/2} + (1.3 \times 10^{-14})\tau^1$  and the floor is  $2.3 \times 10^{-11}$ . The ADEV plot of the lock-in stabilized laser (purple) is shown to have a floor of  $6.6 \times 10^{-13}$  at 30 s with the fit function of  $(7.0 \times 10^{-13})\tau^{-1} + (2.8 \times 10^{-12})\tau^{-1/2} + (1.3 \times 10^{-13})\tau^0 + (6.7 \times 10^{-15})\tau^{1/2} + (8.4 \times 10^{-15})\tau^1$ . The current controller of this laser has a power spectral density of 200 nA/ $\sqrt{\text{Hz}}$ .

of all laser oscillators that is related to the random arrival time of electrons.

## B. Laser intensity stability

Figure 7(a) shows the uncorrected (blue) and corrected (red) intensity measurements of the DF-DAVLL system over a duration of  $\sim 1$  s. It is apparent that vibrational noise in the 1–100 Hz band are strongly suppressed using the intensity stabilization feedback loop shown in Fig. 2 and the corresponding stabilization circuit shown in Fig. 3. Figure 7(a) shows that the standard deviation of the laser intensity fluctuations is reduced by a factor of  $\approx 3$  if the feedback loop is engaged. The noise suppression in this frequency band is also evident from the uncorrected (blue) and corrected (red) power spectral density curves shown in Fig. 7(b). These data show that vibrational resonances in the 10–30 Hz range, which are attributed to the sub-Hertz platform discussed in Sec. II B, can be suitably suppressed. We note that this feedback scheme is also effective in suppressing the intensity noise from the TA due to the flow of cooling water.

## C. Comparative measurements of MOT temperature

In this subsection, we compare the MOT temperature measurements obtained using the home-built laser system stabilized using the modulation-free DF-DAVLL technique with temperature measurements using a commercial ECDL stabilized by a lock-in amplifier. We calibrate the voltage fluctuations from the commercial laser system into frequency excursions by systematically increasing the modulation amplitude. The results are illustrated in Fig. 8. The frequency to voltage conversion is obtained by first converting the

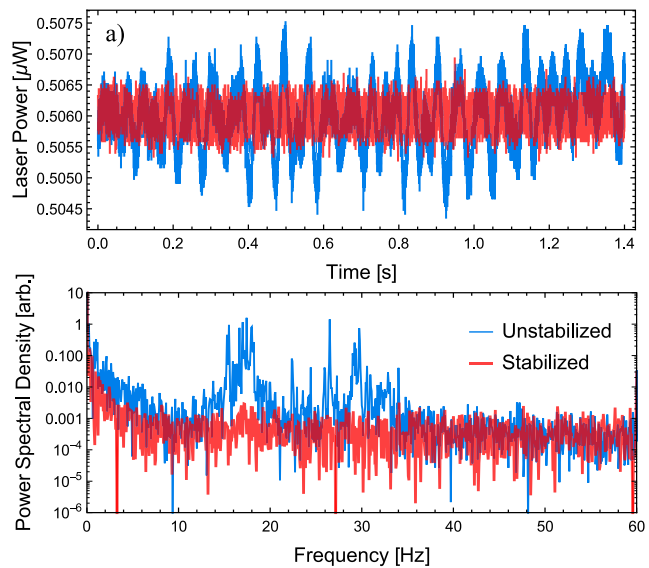


**FIG. 7.** Effect of laser intensity stabilization. (a) Laser intensity variations with (red) and without (blue) feedback. (b) Power spectral density of laser intensity with (red) and without (blue) feedback showing the effect of suppressing acoustic vibrations.

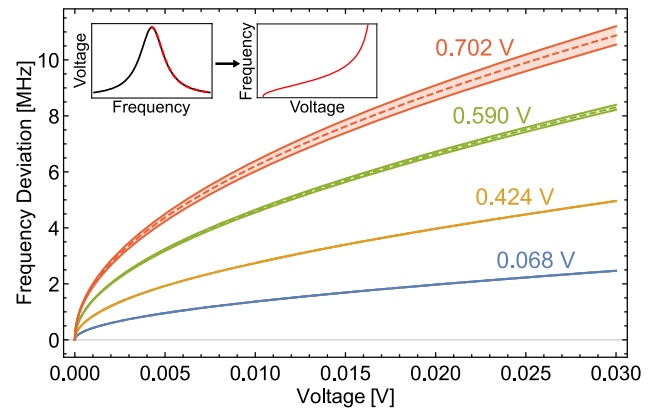


**FIG. 8.** Calibration of laser frequency excursions. The excursions are increased by increasing the modulation amplitude.

horizontal axis of our spectroscopy signal from time to frequency based on the known hyperfine splittings.<sup>52</sup> In Fig. 8, the upper left-hand inset shows a fit to a Lorentzian saturated absorption line shape. The frequency as a function of the voltage is obtained by inverting the right half of this graph as shown in the inset on the right. The main panel shows the frequency deviation from the lock point for a variety of modulation amplitudes. For each modulation amplitude, the calibration curves shown in Fig. 8 are used to convert the laser lock stability to a frequency excursion. In this manner, it is possible to systematically change the linewidth of the laser and investigate its influence on the MOT temperature.

In Fig. 9, we record the cloud expansion as a function of release time from the MOT along two perpendicular axes using a single

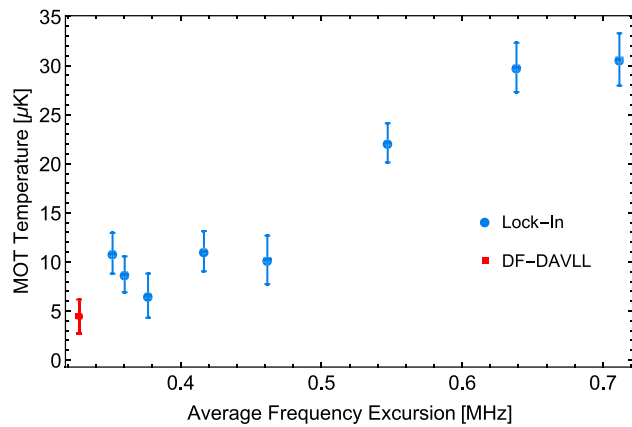


**FIG. 9.** Comparative MOT temperature using lock-in stabilized seed laser (blue) and modulation-free laser system (red). The modulation amplitude of the lock-in stabilized laser was increased to change the effective linewidth resulting in higher temperatures.

CCD camera. For these experiments, the atoms are cooled below the Doppler limit using polarization gradient cooling as described in our previous work.<sup>51</sup> Each temperature measurement relies on photographing the cloud expansion for  $\approx 30$  release times ranging up to 50 ms and averaging over 3 repetitions at each release time. The final temperature was determined by averaging the results of three such datasets. The average temperature along the two axes is plotted as a function of the modulation amplitude, which has been converted to a frequency excursion based on the lock signal. The data (blue points) show that there is a systematic increase in the MOT temperature measured with the lock-in stabilized laser if the modulation amplitude is increased. For the smallest possible modulation amplitude at which the laser remains locked over the data acquisition time, we obtain typical MOT temperatures in the range of 7–11  $\mu\text{K}$ . However, the temperature obtained with the modulation-free DF-DAVLL locked laser system is consistently lower (4.5  $\mu\text{K}$ ) as

shown by the red point on the graph. This limit appears to be connected with the current noise as shown in Fig. 6. It is also evident that the difference in temperature between the two laser systems can be observed within the data acquisition time of 5 min for each data point. These results suggest that modulation-free laser locks have inherent advantages, such as limiting the cloud expansion in atom interferometry experiments. We conclude by noting that the biggest impact on MOT temperature relates to the frequency stability of the laser systems.

#### D. Performance of radio frequency synthesizer

In this subsection, we present results on the stability, tunability, tuning range, and power stability of the dual-output RF synthesizer. Figure 10(a) shows the ADEV of the mixed down and low-pass filtered signal in Fig. 5 monitored using a frequency counter with a resolution of 1  $\mu\text{Hz}$ . We find that the ADEV floor is  $9.3 \times 10^{-9}$  at 5500 s, corresponding to stability at the level of 10  $\mu\text{Hz}$ . We also find that white frequency noise is the dominant term based on the polynomial fit.

To test the tunability of the RF synthesizer, the relative detuning,  $\delta$ , is adjusted using the arbitrary waveform generators, and the beat note is monitored on an oscilloscope. Examples of these beat note frequencies are shown in the inset to Fig. 5 and demonstrate tunability from 1 mHz to 1 MHz. Although the arbitrary waveform generators can be tuned in steps as small as 1  $\mu\text{Hz}$ , we are limited by the stability of the output frequency at the level of 10  $\mu\text{Hz}$  as shown by the ADEV floor in Fig. 10(a).

We characterize the frequency response by measuring the RF power level of one of the synthesizer outputs over a tuning range of a few MHz. Due to the use of the bandpass filters centered at 125 MHz, we expect some nonlinearity in the signal amplitude in the vicinity of this central frequency. This nonlinearity is shown in Fig. 10(b) (blue). This variation can be problematic for atom interferometry experiments since the synthesizer outputs drive AOMs, resulting in systematic laser power fluctuations. It is possible to circumvent this issue by engaging an RF power stabilization feedback loop shown in Fig. 10(c). The implementation is based on the principles of the

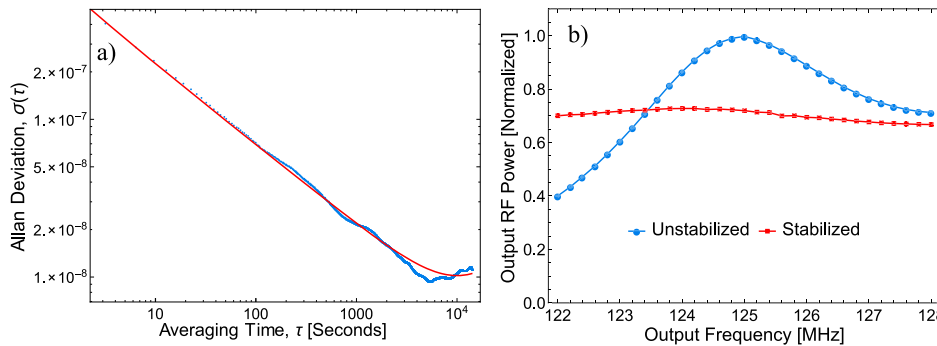


**FIG. 10.** (a) Allan deviation plot characterizing RF synthesizer stability using 1 kHz beat note between the two RF outputs. The ADEV floor is  $9.3 \times 10^{-9}$  at 5500 s and the fit function is  $(1.1 \times 10^{-7})\tau^{-1} + (6.8 \times 10^{-7})\tau^{-1/2} + (7.0 \times 10^{-16})\tau^0 + (1.4 \times 10^{-19})\tau^{1/2} + (3.4 \times 10^{-13})\tau^1$ . (b) Effect of stabilizing the RF power of the synthesizer outputs. Blue shows without stabilization and red shows with stabilization. An error bar representing the standard deviation of the RF power has a typical value of 0.001, which is smaller than the size of the points. (c) Feedback loop for RF power stabilization with the stabilization circuit described in Fig. 3 reconfigured to receive an input from an RF power detector.

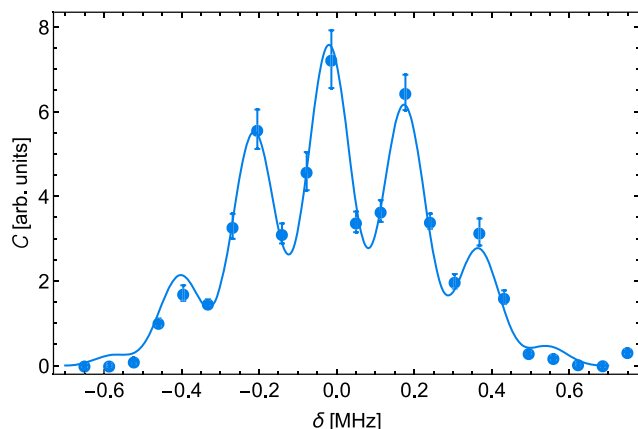


**FIG. 11.** Two-pulse velocimeter signal. The figure shows coherently backscattered free induction decay signal that is proportional to the contrast,  $C$ , of an optical lattice in a sample of laser-cooled atoms. The Ramsey spectrum results from the interaction of two temporally separated composite excitation pulses consisting of counter-propagating traveling waves with a relative detuning  $\delta$ . This relative detuning is imprinted with the stability of the synthesizer of  $\sim 10 \mu\text{Hz}$ .

feedback loop used for laser intensity stabilization. For this application, the circuit described in Fig. 3 is repurposed by deriving the input from an RF powermeter (response time of  $\approx 1 \mu\text{s}$ ) so that a correction is applied to the VCA illustrated in Fig. 10(c). The RF power drop due to this correction is compensated by an RF amplifier that is matched with the entire tuning range. Figure 10(b) shows the stabilized RF power (red) over the  $\sim 6 \text{ MHz}$  tuning range.

The specifications of this synthesizer are more than adequate for the cold-atom velocimeter and gravimeter experiments demonstrated in our recent work.<sup>26–28</sup> Here, the relative detuning between the excitation beams derived from a common laser needs to be varied over a range of 1 MHz for the velocimeter and 1 kHz for the gravimeter with the smallest step size being 1 Hz. The representative data from a two-pulse velocimeter obtained with this synthesizer are shown in Fig. 11. Here, a Ramsey fringe pattern is written on the spectrum of coherently backscattered radiation from a laser-cooled sample of rubidium atoms. In these experiments, the center-of-mass (com) velocity of the sample is directly related to the frequency resolution of the Ramsey fringe. As a result of the tunability of the synthesizer, the velocity of the com of the falling cloud can be determined with a sensitivity of  $600 \mu\text{m/s}$  by determining the line shape center of the Ramsey fringe.<sup>26</sup> Similarly, this synthesizer has been used to measure gravitational acceleration with a sensitivity of  $\approx 1 \text{ ppm}$  using a two pulse frequency domain echo interferometer.<sup>28</sup> We conclude that the biggest impact on these atom interferometric measurements relates to the stability of the relative detuning between excitation beams produced by the RF synthesizer. However, the absolute frequency stability is determined by the quality of the laser locks. Since the repetition rate of the experiment is 1 Hz and the data acquisition time can extend to several minutes, laser intensity stabilization also contributes to the quality of the data.

#### IV. CONCLUSIONS

We have realized a versatile and inexpensive home-built laser system that has the requisite frequency stability for

wide-ranging experiments in precision metrology. The laser system uses a modulation-free frequency stabilization scheme that systematically lowers the temperature of cold atoms. The control electronics include an intensity stabilization feedback loop that is effective in suppressing the effects of table resonances. We have also developed a dual-output RF synthesizer with a stability of  $10 \mu\text{Hz}$ , a tuning range of several MHz, and a step size limited by the stability that can be integrated with this laser system to realize cold-atom velocimeters and gravimeters.

#### ACKNOWLEDGMENTS

This work was supported by the Canada Foundation for Innovation, Ontario Innovation Trust, Ontario Centers of Excellence, U.S. Army Research Office (Grant No. W911NF-12-10564), Natural Sciences and Engineering Research Council of Canada, York University, and the Helen Freedhoff Memorial Fund. We also acknowledge helpful discussions with Louis Marmet of York University.

#### AUTHOR DECLARATIONS

##### Conflict of Interest

The authors have no conflicts to disclose.

#### Author Contributions

**J. Randhawa:** Conceptualization (equal); Data curation (equal); Formal analysis (equal); Methodology (equal); Software (equal); Visualization (equal); Writing – original draft (equal); Writing – review & editing (equal). **G. Carlse:** Conceptualization (supporting); Data curation (supporting); Formal analysis (supporting); Methodology (equal); Software (equal); Visualization (supporting); Writing – review & editing (equal). **M. B. Llaguno:** Data curation (supporting); Writing – review & editing (equal). **J. Cuzzupoli:** Data curation (supporting); Writing – review & editing (equal). **E. Chomen Ramos:** Visualization (supporting); Writing – review & editing (equal). **T. Vacheresse:** Visualization (supporting); Writing – review & editing (equal). **A. Pouliot:** Software (equal); Writing – review & editing (equal). **A. Kumarakrishnan:** Conceptualization (equal); Funding acquisition (equal); Supervision (equal); Visualization (equal); Writing – original draft (equal); Writing – review & editing (equal).

#### DATA AVAILABILITY

The data that support the findings of this study are available from the corresponding author upon reasonable request.

#### REFERENCES

- 1 K. DeRose, T. Deshpande, Y. Wang, and T. Kovachy, *Opt. Lett.* **48**, 3893 (2023).
- 2 M. H. Goerz, M. A. Kasevich, and V. S. Malinovsky, *Atoms* **11**, 36 (2023).
- 3 J. Glick, Z. Chen, T. Deshpande, Y. Wang, and T. Kovachy, *AVS Quantum Sci.* **6**, 014402 (2024).
- 4 Z. Chen, G. Louie, Y. Wang, T. Deshpande, and T. Kovachy, *Phys. Rev. A* **107**, 063302 (2023).
- 5 M. Kim, R. Notermans, C. Overstreet, J. Curti, P. Asenbaum, and M. A. Kasevich, *Opt. Lett.* **45**, 6555 (2020).

- <sup>6</sup>C. Deppner, W. Herr, M. Cornelius, P. Stromberger, T. Sternke, C. Grzeschik, A. Grote, J. Rudolph, S. Herrmann, M. Krutzik *et al.*, *Phys. Rev. Lett.* **127**, 100401 (2021).
- <sup>7</sup>H. Müntinga, H. Ahlers, M. Krutzik, A. Wenzlawski, S. Arnold, D. Becker, K. Bongs, H. Dittus, H. Duncker, N. Gaaloul *et al.*, *Phys. Rev. Lett.* **110**, 093602 (2013).
- <sup>8</sup>H. C. Beica, A. Pouliot, A. Carew, A. Vorozcova, N. Afkhami-Jeddi, T. Vacheresse, G. Carlse, P. Dowling, B. Barron, and A. Kumarakrishnan, *Rev. Sci. Instrum.* **90**, 085113 (2019).
- <sup>9</sup>C. Affolderbach and G. Milet, *Rev. Sci. Instrum.* **76**, 073108 (2005).
- <sup>10</sup>A. S. Arnold, J. S. Wilson, and M. G. Boshier, *Rev. Sci. Instrum.* **69**, 1236 (1998).
- <sup>11</sup>M. G. Littman and H. J. Metcalf, *Appl. Opt.* **17**, 2224 (1978).
- <sup>12</sup>S. Stry, S. Thelen, J. Sacher, D. Halmer, P. Hering, and M. Mürtz, *Appl. Phys. B* **85**, 365 (2006).
- <sup>13</sup>T. P. Dinneen, C. D. Wallace, and P. L. Gould, *Opt. Commun.* **92**, 277 (1992).
- <sup>14</sup>B. Dahmani, L. Hollberg, and R. Drullinger, *Opt. Lett.* **12**, 876 (1987).
- <sup>15</sup>H. Chang, K. Myneni, D. D. Smith, and H. R. Liaghati-Mobarhan, *Rev. Sci. Instrum.* **88**, 063101 (2017).
- <sup>16</sup>W. Lewoczko-Adamczyk, C. Pyrlik, J. Häger, S. Schwertfeger, A. Wicht, A. Peters, G. Erbert, and G. Tränkle, *Opt. Express* **23**, 9705 (2015).
- <sup>17</sup>Q. Lin, M. A. Van Camp, H. Zhang, B. Jelenković, and V. Vuletić, *Opt. Lett.* **37**, 1989 (2012).
- <sup>18</sup>D. Singh, H. Yadav, K. Jain, M. Dangi, and B. Santra, *Rev. Sci. Instrum.* **96**, 073001 (2025).
- <sup>19</sup>X. Baillard, A. Gauguet, S. Bize, P. Lemonde, P. Laurent, A. Clairon, and P. Rosenbusch, *Opt. Commun.* **266**, 609 (2006).
- <sup>20</sup>M. Gilowski, C. Schubert, M. Zaiser, W. Herr, T. Wübbena, T. Wendrich, T. Müller, E. M. Rasel, and W. Ertmer, *Opt. Commun.* **280**, 443 (2007).
- <sup>21</sup>Stanford Research Systems, Model PRS10 Rubidium Frequency Standard, 2015.
- <sup>22</sup>A. Pouliot, E. Chomen Ramos, G. Carlse, T. Vacheresse, J. Randhawa, L. Marmet, A. Kumarakrishnan, J. Klos, and E. Tiesinga, *Phys. Rev. A* **111**, 033108 (2025).
- <sup>23</sup>A. Pouliot, G. Carlse, H. C. Beica, T. Vacheresse, A. Kumarakrishnan, U. Shim, S. B. Cahn, A. Turlapov, and T. Sleator, *Phys. Rev. A* **103**, 023112 (2021).
- <sup>24</sup>H. C. Beica, A. Pouliot, P. Dowling, A. Carew, T. Vacheresse, G. Carlse, L. Marmet, and A. Kumarakrishnan, *Phys. Rev. A* **101**, 033408 (2020).
- <sup>25</sup>G. Carlse, K. B. Borsos, H. C. Beica, T. Vacheresse, A. Pouliot, J. Perez-Garcia, A. Vorozcova, B. Barron, S. Jackson, L. Marmet, and A. Kumarakrishnan, *Phys. Rev. Appl.* **14**, 024017 (2020).
- <sup>26</sup>G. Carlse, J. Randhawa, E. Ramos, T. Vacheresse, A. Pouliot, and A. Kumarakrishnan, *Phys. Rev. A* **111**, L021304 (2025).
- <sup>27</sup>G. Carlse, J. Randhawa, A. Pouliot, T. Vacheresse, E. Ramos, and A. Kumarakrishnan, *Proc. SPIE* **13392**, 1339204 (2025).
- <sup>28</sup>G. Carlse, J. Randhawa, A. Pouliot, E. Ramos, T. Vacheresse, and A. Kumarakrishnan, *Phys. Rev. A* **112**, L061302 (2025).
- <sup>29</sup>K. L. Corwin, Z.-T. Lu, C. F. Hand, R. J. Epstein, and C. E. Wieman, *Appl. Opt.* **37**, 3295 (1998).
- <sup>30</sup>B. Chéron, H. Gilles, J. Hamel, O. Moreau, and H. Sorel, *J. Phys. III* **4**, 401 (1994).
- <sup>31</sup>J. I. Kim, C. Y. Park, J. Y. Yeom, E. B. Kim, and T. H. Yoon, *Opt. Lett.* **28**, 245 (2003).
- <sup>32</sup>G. Wasik, W. Gawlik, J. Zachorowski, and W. Zawadzki, *Appl. Phys. B* **75**, 613 (2002).
- <sup>33</sup>T. Petelski, M. Fattori, G. Lamporesi, J. Stuhler, and G. M. Tino, *Eur. Phys. J. D* **22**, 279 (2003).
- <sup>34</sup>G.-W. Choi and H.-R. Noh, *J. Phys. B: At., Mol. Opt. Phys.* **48**, 115008 (2015).
- <sup>35</sup>M. L. Harris, S. L. Cornish, A. Tripathi, and I. G. Hughes, *J. Phys. B: At., Mol. Opt. Phys.* **41**, 085401 (2008).
- <sup>36</sup>M. Pichler and D. C. Hall, *Opt. Commun.* **285**, 50 (2012).
- <sup>37</sup>R. Giannini, E. Breschi, C. Affolderbach, G. Bison, G. Milet, H.-P. Herzig, and A. Weis, *Proc. SPIE* **6604**, 66040L (2007).
- <sup>38</sup>C. Mok, M. Weel, E. Rotberg, and A. Kumarakrishnan, *Can. J. Phys.* **84**, 775 (2006).
- <sup>39</sup>M. Levenson, *Introduction to Nonlinear Laser Spectroscopy 2e* (Elsevier, 2012).
- <sup>40</sup>K. Sowka, M. Weel, S. Cauchi, L. Cockins, and A. Kumarakrishnan, *Can. J. Phys.* **83**, 907 (2005).
- <sup>41</sup>T. W. Hänsch, I. S. Shahin, and A. L. Schawlow, *Phys. Rev. Lett.* **27**, 707 (1971).
- <sup>42</sup>T. A. Savard, K. M. O'hara, and J. E. Thomas, *Phys. Rev. A* **56**, R1095 (1997).
- <sup>43</sup>A. Pouliot, H. C. Beica, A. Carew, A. Vorozcova, G. Carlse, and A. Kumarakrishnan, *Proc. SPIE* **10514**, 105140S (2018).
- <sup>44</sup>X. H. Qi, L. Yi, Q. L. Ma, D. W. Zhou, X. J. Zhou, and X. Z. Chen, *Appl. Opt.* **48**, 4370 (2009).
- <sup>45</sup>F. C. Cruz, M. C. Stowe, and J. Ye, *Opt. Lett.* **31**, 1337 (2006).
- <sup>46</sup>Y. Wang, K. Wang, E. F. Fenton, Y.-W. Lin, K.-K. Ni, and J. D. Hood, *Opt. Express* **28**, 31209 (2020).
- <sup>47</sup>F. Tricot, D. H. Phung, M. Lours, S. Guérandel, and E. De Clercq, *Rev. Sci. Instrum.* **89**, 113112 (2018).
- <sup>48</sup>D. I. Kim, H.-G. Rhee, J.-B. Song, and Y.-W. Lee, *Rev. Sci. Instrum.* **78**, 103110 (2007).
- <sup>49</sup>E. Davidson, I. Chan, B. Barrett, C. Mok, A. Carew, and A. Kumarakrishnan, in *Bulletin of the Canadian Undergraduate Physics Conference*, 2010.
- <sup>50</sup>A. Vorozcova, M. Weel, S. Beattie, S. Cauchi, and A. Kumarakrishnan, *J. Opt. Soc. Am. B* **22**, 943 (2005).
- <sup>51</sup>G. Carlse, A. Pouliot, T. Vacheresse, A. Carew, H. C. Beica, S. Winter, and A. Kumarakrishnan, *J. Opt. Soc. Am. B* **37**, 1419 (2020).
- <sup>52</sup>D. Steck, Rubidium 85 D line data, 2023, available at <https://steck.us/alkalidata/>, version 2.3.2.